Lawrence Berkeley National Laboratory
Recent Work

Title
EROSION OF HARD METAL COATINGS

Permalink
https://escholarship.org/uc/item/5ct0g0rc

Author
Levy, A.

Publication Date
1982-10-01

Lawrence Berkeley Laboratory

UNIVERSITY OF CALIFORNIA

Materials & Molecular Research Division

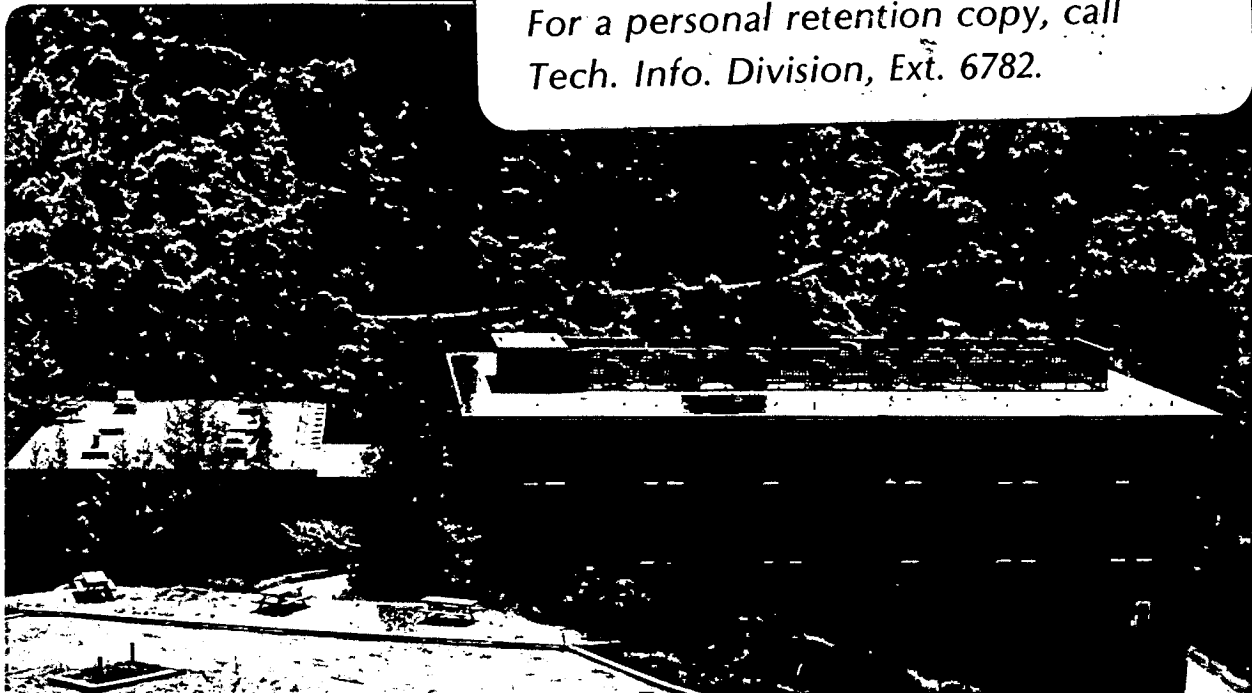To be presented at the 1983 Meeting of TMS/AIME, Atlanta, GA, March 6-10, 1983

EROSION OF HARD METAL COATINGS

A. Levy, T. Bakker, E. Sholz, and M. Azadabeh

October 1982

DISCLAIMER

EROSION OF HARD METAL COATINGS

A. Levy, T. Bakker, E. Sholz, M. Azadabeh

Materials and Molecular Research Division
Lawrence Berkeley Laboratory
University of California
Berkeley, California 94720

-1-

ABSTRACT

The use of protective coatings on components in fossil fuel energy
processes to provide thermal insulation, corrosion resistance and/or
wear resistance is becoming more prevalent. In those applications where
small, erosive particles occur in the environment, such as in the use of
pulverized coal, erosion behavior of the coating becomes an important de-
sign consideration. The erosion of several protective, hard metal type
coatings and monolithic inserts by particles entrained in an air blast
has been investigated. SiC, Si_3N_4, tungsten carbide, and a series of
nickel-chromium-boron alloys were tested at room temperature. The mater-
ials were fabricated by chemical vapor deposition, flame spraying, plasma
arc spraying, detonation gun spraying, melting and brazing, and hot press-
ing. The effects of composition, morphology, method of fabrication, thick-
ness and surface texture on erosion behavior are discussed. The mechanisms
of erosion for the different materials are defined and compared.

It was determined that the materials had a wide range of erosion resist-
ance with the fine grain size and minimum porosity materials having the low-
est erosion rates. All of the materials tested eroded in a brittle manner
with essentially no relationship to hardness.

INTRODUCTION

The wear resistance requirements of some of the components in the emerging energy systems necessitates the use of hard materials of the refactory hard metal family, i.e., carbides, nitrides, borides, silicides, to serve at the wear surface. They are used either as deposited coatings on structural metal surfaces or as separately fabricated inserts that are assembled into a structural metal retaining area. There has been considerable study of the wear behavior of carbides, nitrides and borides in rubbing and sliding wear and in abrasive wear. However, there has been very little research conducted to determine their resistance to wear by erosive particles directed at the surface by a gas stream. In several of the newer energy conversion and utilization systems, particularly those that use coal, the mechanism of erosive wear is an active one that must be considered.

The purpose of this investigation was to determine the basic erosion behavior of several of the most promising refactory hard metal coatings and bodies that are currently either in development or commercial use. A representative group of materials was obtained from a few of the suppliers of hard surface materials and tested at room temperature in an air blast tester. The materials selected were meant to be a sample and not a definitive representation of all of this type of material available. The tests were done at room temperature only to establish an initial basis for understanding the nature of the erosion process and not to attempt to simulate any regime of service conditions. With this screening work completed, the continuing effort will incorporate additional materials and test conditions more nearly simulating service conditions.

EXPERIMENTAL CONDITIONS

Flat, rectangular specimens of the order of 3cm x 2cm x 1/2cm were used. Table 1 lists the materials tested. Since several of the materials tested are still in development or initial production applications, their proprietary nature precludes a detailed description of their composition, structure or method of processing.

The specimens were placed in an air blast tester[1] and eroded incrementally with up to 280gm of 200μm, angular SiC particles carried in an air stream at 30mps (100fps) at room temperature. The velocity was determined using a rotating disc method.[2] The angle of impingement between the direction of the particles out of the nozzle and the flat target surface was α=30°, 60°, and 90°. Total test time ranged from 8 min. to 15 min. (approximately 5 sec/gram) depending upon when a steady state erosion rate was reached. A steady state erosion rate is defined as the condition of the target surface where each succeeding batch of particles causes the same amount of weight loss of the specimen as the previous batch.

The specimens were blasted with small amounts of particles in each erosion increment that were increased as the steady state of erosion was approached, as can be seen by the weight loss curves. Weighing was done on a balance which indicated to 0.1 mg.

Scanning electron microscopy (SEM) was used to examine the steady-state erosion surfaces. On some of the specimens x-ray diffraction and scanning Auger microscopy (SAM) were used to determine the chemistry of the eroded surfaces. Fracture analysis and micro-hardness determinations were used to aid in the interpretation of the CNTD SiC coatings tested.

RESULTS

The steady state erosion rate of each type of material tested at $\alpha= 30°$ and 90° impingement angles is shown in Fig. 1. Because of the wide variation in density, the bar chart is based on volume of material removed per gram of erodent rather than weight of material removed. A wide range of performance occurred for the group of test materials. In all instances the materials eroded more at $\alpha= 90°$ than at $\alpha= 30°$ which is typical of brittle type materials. For comparison purposes mild steel erosion rates are also presented in Fig. 1.

Silicon Carbide

There was a wide variation in the erosion behavior of silicon carbide depending on its type, fabrication method and source. A more detailed look at the variation in just one version of SiC, the chemically vapor deposited, continuous nucleation thermal deposition (CNTD) coatings[3] is shown in Table 2. The coatings varied as a function of processing conditions and silicon-silicon carbide contents. It can be seen that there was well over 1 order of magnitude difference in erosion rate as a function of coating hardness and an order of magnitude difference between the rates at impingement angles of $\alpha= 30°$ and 90°. Steady state erosion occurred after considerably more particles had impacted the surface at $\alpha= 30°$, 200g, than at $\alpha= 90°$, 20g. At hardnesses greater than 3000 VHN there was very little difference in the erosion rate as a function of hardness. The silicon to carbon ratio measured by SAM was essentially the same for specimens with a hardness $\geq$3000 VHN varying from 49/51 to 51/49. However, the 2400 VHN CNTD SiC has a silicon to carbon ratio of 56/44. Generally the monolithic SiC samples, NC-430 and NC-203, had greater erosion rates than did the vapor deposited CNTD SiC with the exception of the lowest hardness CNTD SiC coating at $\alpha= 90°$.

Figs. 2 and 3 plot the incremental erosion rates for the several CNTD SiC materials for $\alpha = 30°$ and $\alpha = 90°$. The curves of CNTD SiC at 2400 VHN were not plotted because they were an order of magnitude higher than the others. The curves show a typical shape for many brittle materials. There is a rapid rise in erosion rate at the beginning of the test to a high rate, followed by a decreasing rate upon further erosion until a steady state rate is reached. There appears to be no pattern for the position of each material's curve relative to the others.

A peculiar phenomina occurred at $\alpha = 90°$ only in the CNTD SiC coatings that was a function of coating thickness. If the coating was less than about 90 microns thick, it failed catastrophically after only a few grams of particles had struck the surface (<30g), exposing the graphite substrate. Fig. 4 shows a specimen with a coating thickness of 4 microns that was eroded at $\alpha = 90°$ and failed in this manner. If the coatings were greater than 90 microns, they did not erode through to the substrate until hundreds of grams of particles had impacted them. The coatings successfully tested were in the 3 - 8 mils thickness range.

75 - 200 μm

Another phenomina is shown in Fig. 5. On some coatings, grooving was observed near the coating-substrate interface. It can be seen in Fig. 5 that the grooves were associated with a narrow region of much larger grains than the general grain size of the coating. There may have also been some porosity in the larger grain area. Both larger grains and the porosity would cause preferential higher erosion rates where they occurred resulting in the macroscopic appearing grooves. The chipping away of the fine grains on either side of the grooves can be seen in the larger magnification photo in Fig. 5.

Tungsten Carbide

Figs. 6 and 7 show the incremental erosion curves of the LW-5 and LW-15 detonation gun sprayed tungsten carbide coatings on a stainless

steel substrate at α= 90°. The erosion rates were markedly lower at
α= 30° as can be seen in the bar chart, Fig. 1. The curves are similar
in shape to that of the CNTD SiC, but have more gradual slope down to their
steady state erosion rate. The LW-5 required 35 grams of particles to
reach steady state while the LW-15 material reached steady state in only
15 grams. The 3200 VHN CNTD SiC took only 10 gm to reach steady state
erosion and the 2400 VHN CNTD SiC reached it in 5 gm of particles at α= 90°.
The time to reach steady state is a characteristic erosion behavior property
of materials. It appears to relate to the level of steady state erosion;
the longer it takes to reach steady state erosion, the lower is the final
erosion rate in the case of the CNTD SiC and the sprayed WC.

The Kenametal K701 and K703 bodies had erosion rates of 0.063 and
$0.054 cm^3/g$ respectively at α= 90°. These low rates compared to those of the
LW-5 and LW-15 sprayed coatings (0.336 and $0.322 cm^3/g$ respectively at α= 90°)
are related to the morphology of the materials. The pressed and sintered
K701 and K703 specimens were less porous than the sprayed coatings.

Hot Pressed Silicon Nitride and Silicon Carbide

The hot pressed NC-132 silicon nitride and NC-203 silicon carbide
had low rates of erosion at steady state and incremental erosion rate
curves that were different from those of the deposited materials. Figs.
8 and 9 show that the nature of the erosion was one of an increasing ero-
sion rate up to an initial peak rate and then a drop off to a steady state
rate, similar to that which occurs in many ductile metals. Still, their
overall behavior was that of brittle materials.

Nickel - Chromium - Boron Coatings

The erosion tests performed on boride hard metals were carried out on
a series of nickel base alloys containing Cr, Si, Fe and B. The materials
are multi-phase as indicated in Table 3 where the hard metal second phases
are incorporated into the matrix alloy to provide increased wear resistance.

The addition of tungsten carbide particles to further enhance the hardness of one of the alloys was investigated. Three methods of application to a low carbon steel substrate were evaluated. The braze coat specimens were prepared by melting a thin layer of the alloy (greater than 10 mils) and subsequently brazing the layer to the plain carbon steel substrate using braze metal of the same composition. In the case of the braze coats containing $WC-W_2C$ particles, a silver-copper eutectic was used to braze the layer to the substrate. The flame spray and plasma spray processes were done using standard commercial processes.

Table 4 lists the steady state erosion rates of the material systems tested. The specimens were eroded with 200μm diameter size SiC at a velocity of 30mps and an impingement angle of 90°. The base alloys had very similar erosion rates even though there was significant variation in the amount of hard, second phase borides and carbides in them. The microhardness test results are listed in Table 5. They appear to have no relation to the erosion rates.

The principal difference in the erosion of the materials resulted from their method of application to the steel substrate. The least erosion occurred in the melted and brazed on coatings. The flame spray coatings had somewhat more erosion and the plasma spray coatings had the greatest erosion. The flame sprayed AMS-4775 alloy was sprayed on too thin to reach steady state erosion prior to its complete loss from the steel surface. The addition of $WC - W_2C$ hard particles to the braze coated materials markedly increased their erosion rates. The higher carbide contents had the greater erosion rates. The erosion rates listed in Table 4 have been normalized to account for the difference in density between the base alloy and the tungsten carbide particles.

Fig. 10 shows the incremental erosion rates of the AMS-4779 alloy applied by the three processes. The braze coat material behaves in a semi-ductile manner as evidenced by the shape of its curve in Fig. 10. Its erosion rate rises to a peak after a few grams of erodent have impacted it and then decreases to a steady state erosion rate. Both the flame sprayed

and the plasma sprayed coatings behave in a brittle manner. They rapidly reach a high peak erosion rate at the beginning of the test and then the rate decreases rapidly to a low steady state rate.

METALLOGRAPHIC ANALYSIS

The scanning electron microscope (SEM) was used to study the nature of the physical deformation that occurred on each material as the result of the erosion process. Fig. 11 shows scanning electron microscope (SEM) photos of the CNTD silicon carbide coatings' eroded surfaces after steady state conditions were reached at $\alpha=90°$. The uneroded surfaces of the two coatings were essentially alike. After erosion there is a great difference in the appearance of the surface at both lower and high magnifications. The 3200 VHN SiC appears to be eroding by the loss of fine chips of material, representative of a very fine grain size. The 2400 VHN SiC on the right hand side of Fig. 11 is eroding by a mechanism of combined cleavage of crystallites of a considerably larger grain size than that of the harder SiC and some plastic deformation of the material that appears to have a small degree of ductility.

Fig. 12 shows the appearance of the $\alpha= 90°$ eroded surfaces of the 3200 VHN and 2400 VHN CNTD silicon carbide at the time of the peak erosion rate as shown in Fig. 3. It can be seen that considerably more surface has been affected in the 2400 VHN SiC than in the 3200 VHN SiC even though the peak erosion rate of the harder SiC is higher at this early point in the erosion of the two surfaces.

Fig. 13 shows the eroded surfaces of 2400 VHN (top photo) and 4000 VHN (bottom photo) CNTD SiC eroded at $\alpha=30°$. Unlike the specimens eroded at $\alpha= 90°$ (Fig. 11), there appears to be very little difference in the morphology of the softer and harder CNTD SiC surfaces.

A fractographic analysis was made of the CNTD SiC coatings. The specimens were notched on the graphite substrate side to a point near the

coating-substrate interface and then broken by an impact blow which placed the coating in compression. The fractured surfaces were studied using the SEM. Two distinct types of fracture surfaces were observed. Fig. 14, top, shows that the 3500 VHN coating appeared to deposit in two distinct layers, both of which were very fine grained. The somewhat coarser grain appearing region near the coating-substrate interface may be related to the periodic regions of larger grains that caused the grooves shown in Fig. 5. Fig. 14, bottom, shows a single layer coating for the 4000 VHN coating with an apparent overstructure of regions of small grains or pock marks.

Fig. 15 shows higher magnification photos of the fractured surfaces of the 2400, 3000 and 4000 VHN coatings. A fine network of cracks or grain boundaries or areas of high silicon content are seen. Exactly what the dark line appearing network is is not known at this time. The surfaces shown appear to have the same size structure for all three coatings, even though the erosion rates differed significantly, see Table 2. The width of the dark areas appears to vary somewhat in the 4000 VHN coating, and sometimes appears to be oriented in a direction, as in the 3000 VHN coating.

Fig. 16 shows a representative area of the fracture surface at a still higher magnification. It can be seen that the dark lines appear within apparent grains or dimples, beginning to but not completely dividing them into even smaller entities. Fig. 17 shows an area on the fracture surface of the 4000 VHN coating where a wide variation in element size exists as well as considerable difference in the width of the black line divisions. This is a more gross example of the variation in the elemental size of sub-divisions of the fracture surface structure. It appears to be similar to regions of hot tearing in ductile metals.

Fig. 18 shows the steady state erosion surface of the LW-5 tungsten-carbon coating. The appearance of the material at the surface indicates that considerable plastic deformation had occurred along with some lesser amount of brittle fracture or chipping. The degree of plastic deformation

is considerably more than was seen on most of the metal binder content coatings. The nature of the platelets formed is similar to those formed when ductile metals are eroded.

Fig. 19 shows cross sections of the three types of AMS 4779 Ni-B alloy in the as-deposited condition. The differences in the general porosity level directly relates to the erosion rate. The melted and brazed on coating has the least porosity and the lowest erosion rate. The plasma spray coating has the largest random porosity throughout its cross section and the highest erosion rate. The flame sprayed coating has voids between the deposited layers, but essentially no random porosity within individual splats.

DISCUSSION

The erosion behavior of the hard materials tested varied over a relatively wide range as is shown in the bar graph, Fig. 1. The variation in hardness of the various refactory hard metals tested did not relate to the differences in measured erosion rate. Therefore, the erosion rates must be attributed to a combination of characteristics such as composition; amount, type and morphology of the binder material; grain size; crack behavior and other factors which combine to absorb and distribute the kinetic energy of the impacting particles. All of the materials tested at 2 angles had the characteristic erosion behavior of brittle materials, i.e., the erosion rate was greater at the 90° impingement angle than at the more shallow 30° impingement angle. The fact that it took 10 times as many grams of erodent for the CNTD SiC coating to reach steady state erosion at $\alpha = 30°$ than at $\alpha = 90°$ relates to the efficiency of the impinging particles in establishing a crack network in the coating. Particles impacting at $\alpha = 90°$ are much more efficient in cracking the coating.

The role of such binder materials as silicon metal in the SiC material systems and cobalt in the sprayed tungsten carbide materials does not modify

the basic brittle mode of erosion. However, it does modify the mechanism and sensitivity of the material to erosion with the lower silicon content, more intimately mixed silicon-silicon carbide or nitride materials having the best erosion resistance. Since several of the SiC materials tested are highly proprietary and their grain structures very fine, the distribution of silicon in them is not known without further analysis or information from the supplier.

The erosion rates of a ductile metal, 1020 steel, are shown in Fig. 1. The role of ductility in erosion is a significant one. The mild steel has comparable erosion rates to the hard metals even though its hardness is only 150 VHN. In sliding or abrasive type wear the hard metals greatly out-perform the steel.

The very low erosion rate of the $\geq$3000 VHN CNTD SiC compositions is due primarily to the fineness of the distrubution of the binder phase and the small grain size of the four materials in this group. All four materials had about the same grain size, approximately 1000Å. This resulted in material loss by cracking and chipping away of very small pieces. The 2400 VHN CNTD SiC has a considerably larger grain structure and a significantly higher silicon/carbon ratio, indicating that it had more free silicon than the finer grain compositions. These variations resulted in a marked difference in the erosion mechanism, see Figs. 11 and 12, and a considerably higher erosion rate as can be seen in Table 2. The coarse grain, 2400 VHN material appeared to fail by the breaking off of larger crystallites compared to the fine cracking and chipping which occurred in the very fine grained $\geq$3000 VHN CNTD SiC. Scanning Auger Microscopy (SAM) analysis of the 3200 and 2400 VHN CNTD materials also indicated that the 2400 VHN, higher erosion rate material, had considerably higher oxygen content which could also have affected its erosion rate. The effect of grain size on erosion rate was also shown in the grooves that were observed near the coating-substrate interface, Fig. 5. The locally much larger grains eroded at a much higher rate than the main coating body

small grains.

The relatively low erosion rates of the hot pressed silicon carbide and silicon nitride from the Norton Co. also relates to the fine grain size and binder distribution that can be achieved by this type of processing. Hot pressing is generally size limited and is used to produce smaller wear resistant bodies or inserts. The ability of the chemical vapor deposition process to deposit the coating of CNTD SiC on both small and large surfaces with such a fine structure and low erosion rate shows the promise of this method of developing wear resistant material systems for a large variety of applications.

The erosion rate peaks that some of the materials experienced, as shown in Figs. 2 and 3 for the CNTD SiC, is typical of the erosion of more brittle materials. In the work of Zambelli and Levy[4] to determine the erosion behavior of NiO formed on CP nickel, the same type of peaks were observed. They are due to the high initial loss of material in the as-deposited surface layer of the brittle material where more vulnerable crystals of the material protrude from the surface and can be more easily broken off. After the initial loss, the surface has been flattened out considerably and impacting particles must cause cracks that penetrate into the material to separate out pieces of material for removal. This occurs at a considerably lower rate, sharply reducing the erosion rate.

The micro-cracking mechanism accounts for the difference in the shape and peak height of the erosion rate curves for the $\geq$3000 VHN and 2400 VHN CNTD SiC. The smaller grained, more strongly bonded hard material would undergo considerably more initial surface cracking without loss of material than the soft material. Hence, when the crack pattern has been completed in the surface layers and material loss commences, an initial high rate of loss occurs in the hard SiC and a lower initial rate in the soft material. The amount of impacting particles to achieve steady state erosion, i.e., the more particles it takes, the lower is the erosion rate (see data top of pg.6)

also relates to the micro-cracking of the coating.

The rapid failure of the CNTD SiC coatings that were less than 90μm thick probably relates to the depth of cracks that are caused by the impacting particles. This subject is discussed more in ref. 4. The thin coatings could be cracked through by a relatively small amount of particles, resulting in a castastrophic removal once the cracks had penetrated to the substrate.

The erosion rate curves of the detonation gun applied tungsten-carbon coatings LW-5 and LW-15 is similar to that for the 3200 VHN CNTD SiC, but the curves fall off much more gradually to a higher steady state condition because of their different structure and composition. Within the same composition of a material, the more gradual the slope of the curve the steady state erosion, the lower is the steady state erosion rate. However, the comparison does not appear to apply between different materials. The CNTD SiC materials' erosion rates fall off to steady state considerably faster than do the tungsten-carbon coatings; yet are considerably lower. The difference in the erosion mechanism between the CNTD SiC and the LW-5 and 15 materials appears to be that the tungsten-carbon coatings undergo considerably more plastic deformation at the eroding surface than does the CNTD SiC materials.

The hot pressed bodies of silicon carbide, NC-203, and silicon nitride, NC-132, have erosion rate curves that are considerably different from the previously discussed materials. They do reach a peak erosion rate after the initiation of erosion, but undergo a lower but measurable erosion rate prior to reaching the peak rate. In the case of the silicon nitride, the peak rate is very near the steady state erosion rate.

The difference in the erosion rates of the flame sprayed and plasma sprayed Ni-Cr-B coatings is due primarily to the amount of porosity present in the coatings. In ref. 4 Zambelli and Levy determined that erosion rates of brittle behaving materials increase with increasing porosity.

Fig. 19 shows that the plasma sprayed alloy has a greater amount of random porosity than the flame sprayed alloy. The ability of impacting erodent particles to develop stresses around these voids from which cracks are initiated that propagate near parallel to the material surface increases the material removal rates. For brittle materials the erosion depends on the initiation and propagation of cracks. The essence of this mechanism of crack formation at voids and subsequent propagation for ductile metals is discussed in ref. 5.

The marked increase in erosion rate by addition of brittle tungsten-carbide particles to the Ni-B braze coat material is related to the small but significant changes in the ductility of the coatings. In ref. 1 Levy discussed the role of increased ductility in enhancing the erosion resistance of ductile metals. Since the braze coat materials behaved similarily to a ductile metal, albeit they are quite brittle, the addition of the brittle carbide reduced whatever local ductility the AMS-4777 material had, resulting in increased erosion rates. The more $WC-W_2C$ eutectic was added, the higher the erosion rates became, as can be seen in Table 4.

The effect of hardness on the erosion behavior of different base materials is shown by comparing the CNTD SiC with the Ni-Cr-B alloys. From Fig. 1 it can be seen that the 4000 VHN CNTD SiC coatings (Table 2) had about the same erosion resistance as the 439 VHN Ni-Cr-B coating (Table 5). It is in abrasive or sliding wear where there is continuous contact between the materials doing the wear and being worn that hardness directly relates to wear resistance.

Selection of coating systems for particular types of applications must be based on a number of factors. The wide difference in erosion rates (Fig. 1) do not eliminate all but the lowest erosion rate coatings from all applications. If abrasive or sliding wear in addition to erosive wear occurs, than the erosion rate is not the only factor. Good sliding wear resistant materials have different characteristics from good erosive wear resistant

materials. Hardness relates directly to abrasive sliding wear, but
not to erosive wear.

The configurations of parts and the effects of elevated temperature
processes to deposit the coatings on them help to dictate which coatings
are appropriate. Thus the detonation gun W-C coatings require direct ac-
cess to all surfaces to be coated while the chemical vapor deposited (CVD)
coatings have great throwing power into hidden areas. Chemical and physi-
cal compatibility of the deposited coating and the substrate are also im-
portant variables to assure the necessary adherence and stability over the
life of the part. In this regard, coating thickness is important to part
life. If the erosive environment is going to result in a definitive mat-
erial loss rate, then the thickness of the wear resistant coating has to
be sufficient to last the required part life. This may eliminate some
of the processes which tend to deposit thinner coatings such as the CVD
process.

Combined service requirements at elevated temperatures such as thermal
barrier requirements and corrosion resistance in addition to erosion re-
sistance will dictate a particular material. Thus CVD SiC has a higher
potential maximum service temperature than the cobalt bonded W-C coatings,
LW-5 and LW-15. In some localized severe application areas like small
diameter valve seats, solid body inserts such as the hot pressed SiC or
Si_3N_4 are more appropriate than coatings deposited on the wear area sub-
strate metal.

The knowledge developed and reported herein on how much and why var-
ious coating systems erode when subjected to a gas-solid particle stream
can be used to select protective coating systems for specific applications.
The information also has considerable value on indicating to coating devel-
opers and producers what aspects of coating material systems enhance erosion
resistance to aid them in their efforts to produce more protective systems.

CONCLUSIONS

1. There was a comparatively wide variation in the erosion behavior
    of a group of hard metal coating systems and inserts that were deve-
    loped primarily for their wear resistance. The most erosion resistant
    coatings were fine grained CNTD SiC deposited by chemical vapor de-
    position and braze coated AMS4777 Ni-Cr-B alloys.

2. Hardness of the coatings had a minimum effect on their erosion re-
    sistance. Materials with hardnesses ranging from 4000 VHN to 439 VHN
    had the same erosion rates.

3. The primary material characteristics that increased erosion resistance
    were fine grain size and minimum porosity.

4. All of the materials tested at two impingement angles, $\alpha= 30°$ and
    90°, behaved in a brittle manner, i.e., erosion rates were higher at
    $\alpha= 90°$ than $\alpha= 30°$.

5. The coatings generally had a peak incremental erosion rate shortly
    after erosion initiated which rapidly dropped to a lower steady state
    rate. This is probably caused by the initial rough surface of the
    as-deposited coating which presents many protruding crystals to the
    incoming erodent particles that are vulnerable to being knocked off
    the surface. The eroding surface smoothes out as erosion progresses
    and the erosion rate decreases.

6. The fine grained coatings such as the ≥ 3000 VHN CNTD SiC eroded by
    cracking and chipping out of small pieces of material. The coarse
    grained coatings such as the 2400 VHN CNTD SiC eroded by a different
    mechanism that involved removal of elements that reflected their much
    larger grain size.

7. The grooves that occurred near the coating-substrate interface in the erosion of the hard CNTD SiC coatings occurred as the result of the preferential erosion of localized areas of large grains that apparently grew because of an instability in the deposition process that occurs near its initiation.

8. All of the factors that apply must be considered in selecting materials for service in erosion environments, not just their erosion rate.

REFERENCES

1. Levy, A.; "The Solid Particle Erosion Behavior of Steel as a Function of Microstructure;" Wear 68, p 269 - 283; 1981

2. Ruff, W. and Ives, L.; "Measurements of Solid Particle Velocity in Erosive Wear;" Wear 35, p 195; 1975

3. Stiglich, J and Holzle, R.; "Coatings for Elevated Temperature Wear Resistance;" Proceedings of NACE Conference on Corrosion-Erosion-Wear of Materials in Emerging Fossil Energy Systems, Berkeley, California; January 27 - 29, 1982

4. Zambelli, G. and Levy, A.; "Particulate Erosion of NiO Scales;" Wear 68, p 305 - 332; 1981

5. Jahanmir, S. and Levy, A.; "The Effects of Microstructure of Ductile Alloys on Solid Particle Erosion Behavior;" Proceedings AIME-TMS Fall Meeting; Saint Louis, Missouri; October 1978

Table 1

Material Designation	Composition	Substrate	Fabrication Method	Surface Condition	Source
CNTD SiC	Silicon Carbide	Graphite	Chemical vapor deposited	as deposited	San Fernando Laboratories
LW-5	Tungsten Carbide	Stainless Steel	Detonation Gun sprayed	ground	Union Carbide Linde
LW-15	Tungsten Carbide	Stainless Steel	Detonation Gun sprayed	ground	Union Carbide Linde
ROKIDE C	Chromium Oixde	Black iron	Oxy-acetylene sprayed	as sprayed	Norton Co.
NC-132	Silicon Nitride	None	Hot pressed	as pressed	Norton Co.
NC-203	Silicon Carbide	None	Hot pressed	as pressed	Norton Co.
NC-403	High purity silicon carbide + silicon	None	Reaction sintering + densification of slip cast material	as sintered	Norton Co.
K-701	Tungsten Carbide	None	Pressed and sintered	as sintered	Kenametal
K-703	Tungsten Carbide	None	Pressed and sintered	as sintered	Kenametal
AMS 4775	Ni-Cr-B-Fe-Si	Mild steel	Spray Coating and Cladding	GROUND	GTE
AMS 4777	Ni-Cr-B-Fe-Si	Mild steel	Spray Coating and Cladding	GROUND	GTE
AMS 4779	Ni-B-Si	Mild steel	Spray Coating and Cladding	GROUND	GTE

Table II
Steady State Erosion Rates of CNTD SiC

Sample tested	angle	Steady State Erosion Rate x 10^{-4} g/g
CNTD 4000 VHN	90°	0.10
CNTD 3500 VHN	90°	0.10
CNTD 3200 VHN	90°	0.17
CNTD 3000 VHN	90°	0.20
CNTD 2400 VHN	90°	2.50
CNTD 4000 VHN	30°	0.013
CNTD 3500 VHN	30°	0.02
CNTD 3200 VHN	30°	0.036
CNTD 3000 VHN	30°	0.013
CNTD 2400 VHN	30°	0.19

Table III
Nickel-Boron Alloys Wear Resistant Coatings, Claddings

Alloys	Ni	Cr	Si	Fe	B	S.C. g/cc	2nd Phase	2nd Phase Quantities in Microstructure
AMS-4775	73.4	14.3	4.3	4.7	3.3	7.8	Ni-Cr-B, Cr-C	>> 40%
AMS-4777	83.0	7.0	4.0	3.0	3.0	7.97	Ni-Cr-B	> 40%
AMS-4779	94.7	-	3.5	-	1.8	8.38	Ni-B	~ 40%

Table IV
Steady state Erosion Rates of Nickel-Boron Alloy Coatings, Claddings

Materials	Steady State Erosion Rate x 10^{-6} g/cc		
	Braze Coat	Flame Spray	Plasma Spray
AMS-4775	5.13	-	8.85
AMS-4777	5.27	5.90	9.79
AMS-4779	5.37	6.08	6.44
AMS-4777 + 40WT% WC	7.51	-	-
AMS-4777 + 25WT% WC	7.62	-	-
AMS-4777 + 10WT% WC	7.10	-	-

Notes:

1. Data Normalized for density of specimen material WC SG = 16g/cc

2. Tungsten Carbide addition consists of WC and W_2C mixture

3. Steady State Rate after 250g particles except 130g for AMS4777 + 40WT% WC

4. Alloy Coatings >10 mils Thick; Alloy + WC Coatings 4mils Thick

5. Alloys Self Brazed; Alloys + WC Brazed with AG-Cu Eutectic

6. AMS-4775 Flame Spray Coating Too Thin

TABLE V
Nickel-Boron Alloys Microhardness

Material	Microhardness in VHN		
	Braze Coat	Flame Spray	Plasma Spray
AMS-4775	552	606	538
AMS-4777	439	542	525
AMS-4779	438	402	323
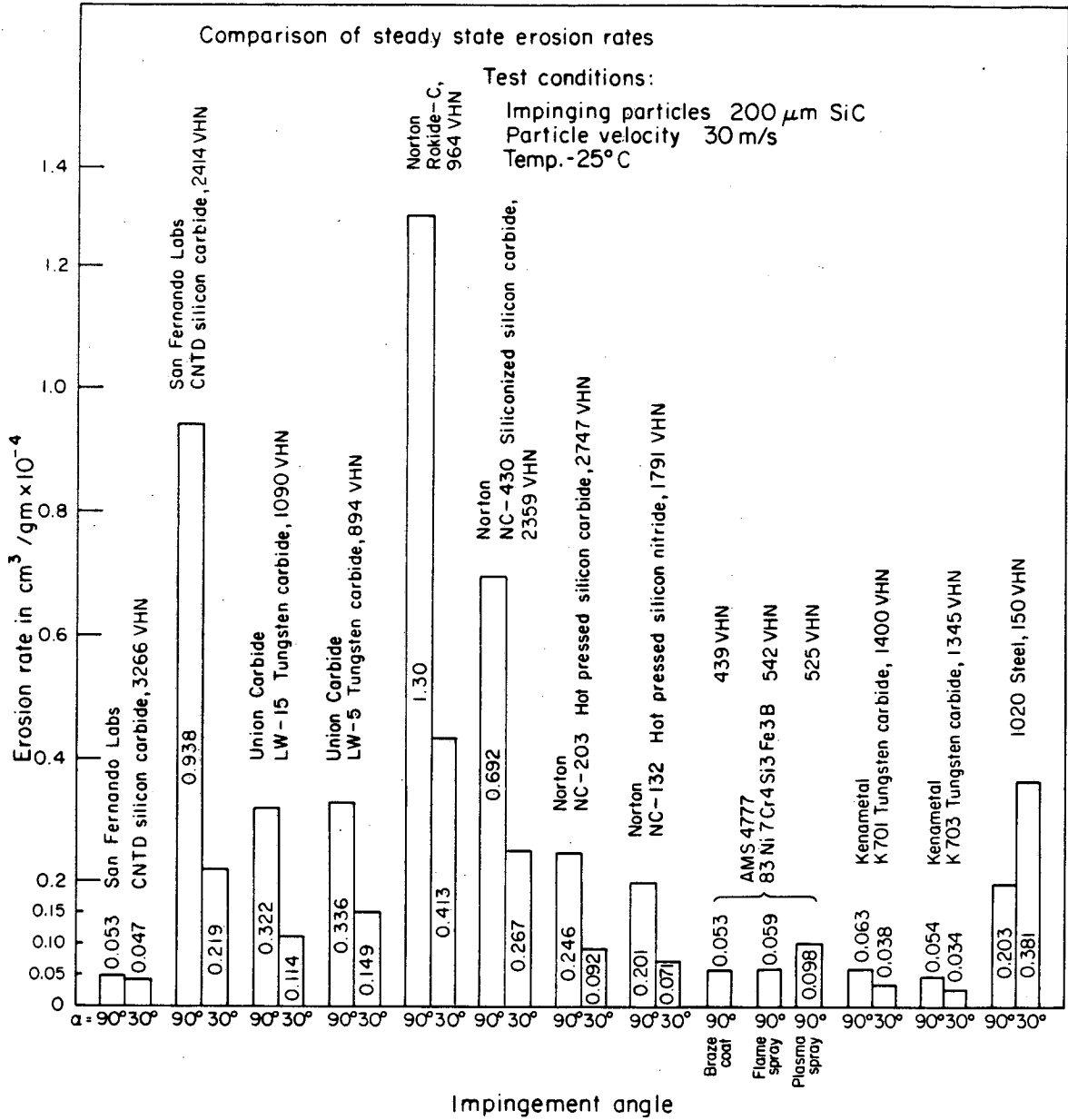
Fig.1 Bar chart of steady state
erosion rate of each material

Erosion rate vs. total particle weight for CNTD SiC coatings
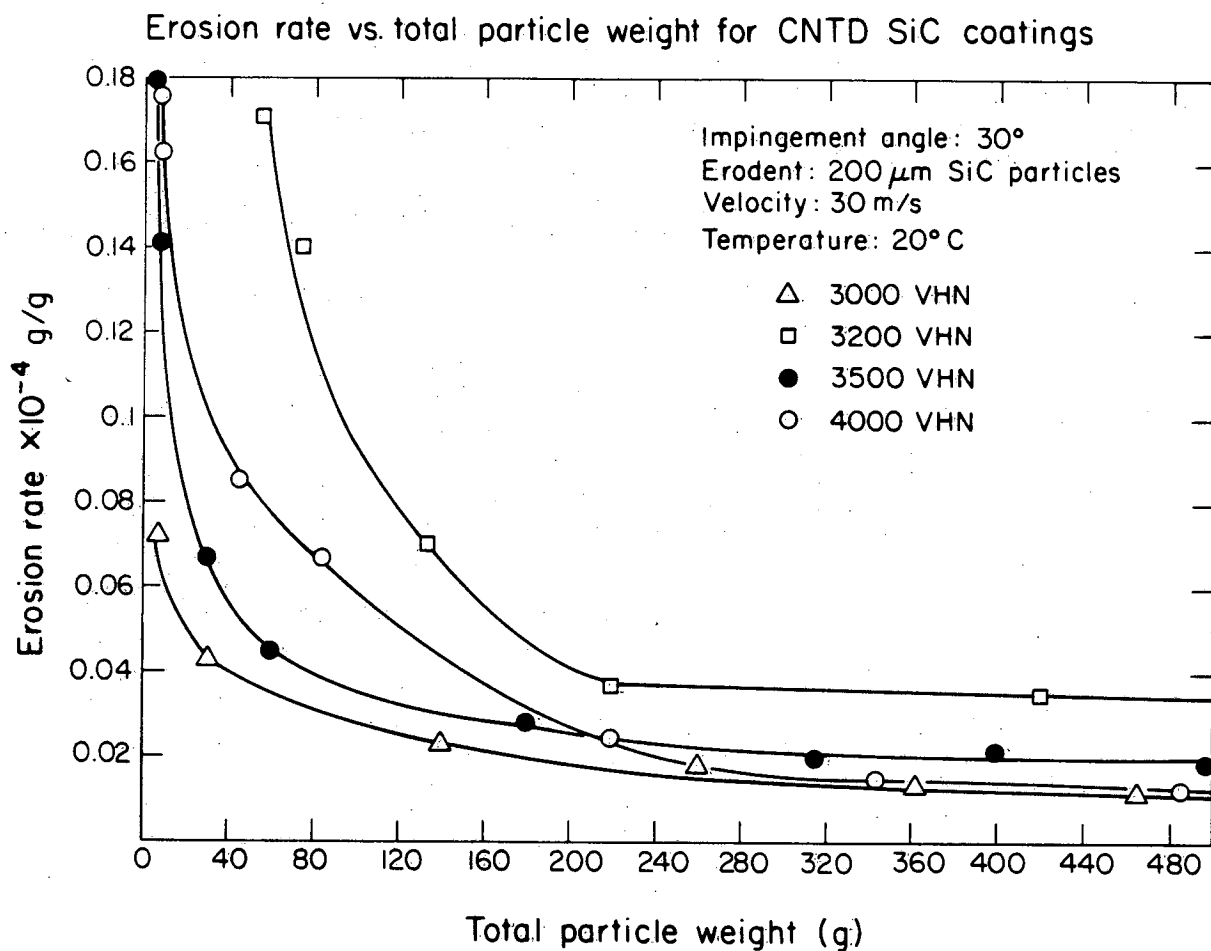
Fig.2 Incremental erosion rate of CNTD
SiC at $\alpha = 30^{\circ}$
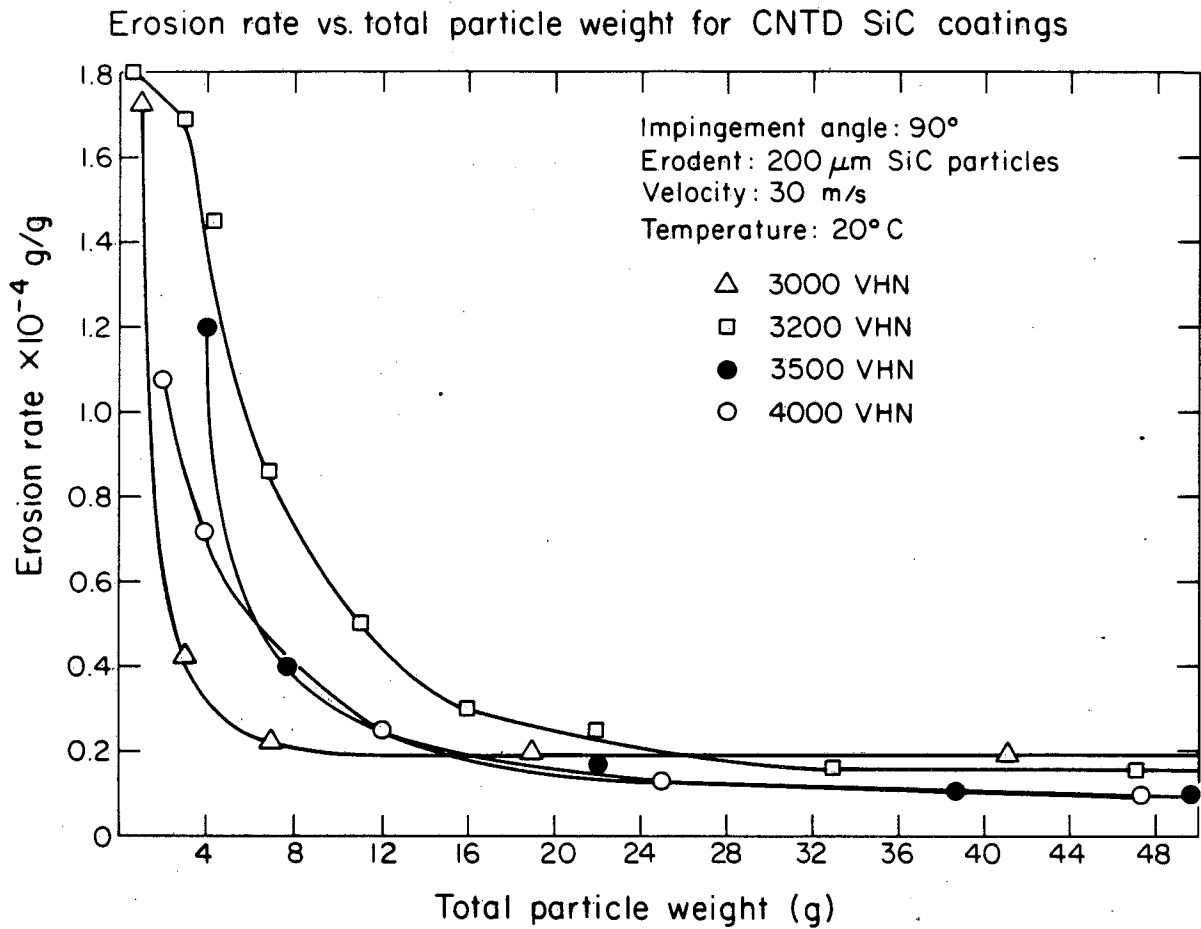
Fig.3 Incremental erosion rate of CNTD
SiC at α= 90°
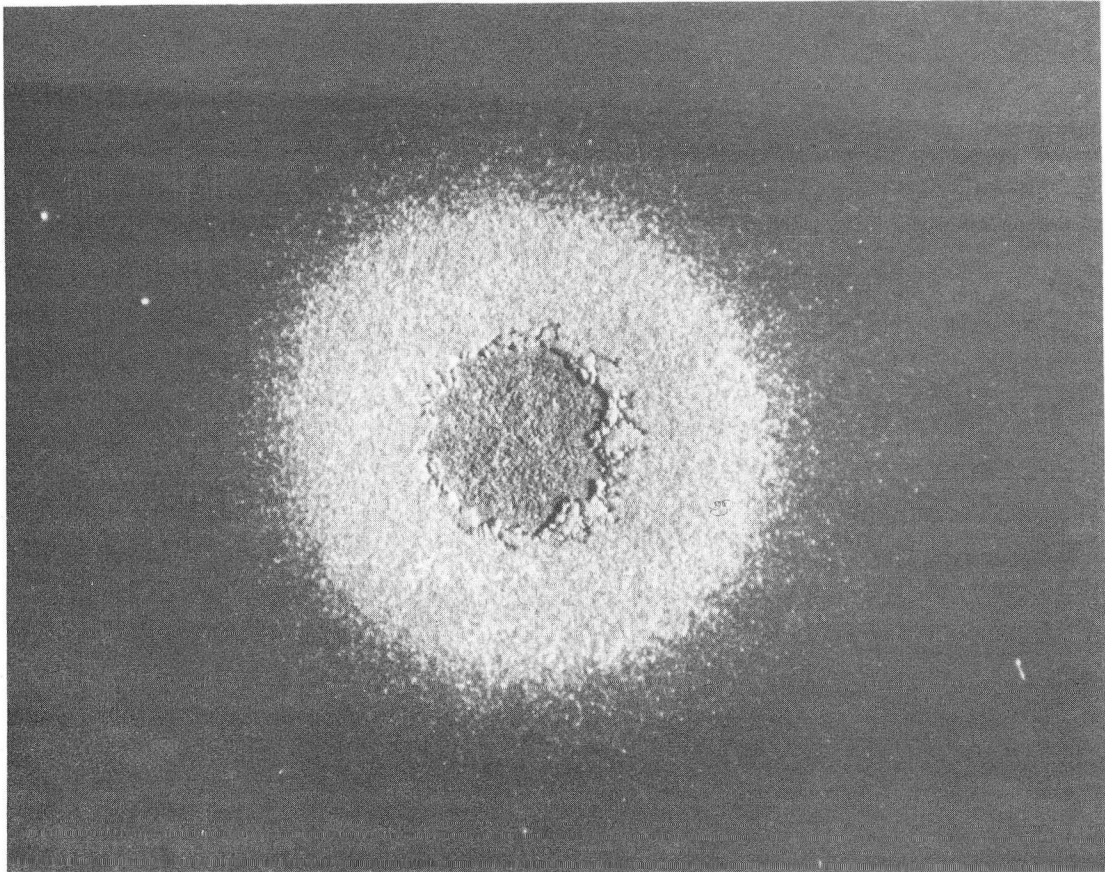
2400 VHN CNTD SIC

2000µm

XBB 8210-9438

FIG.4 Catastrophically Failed CNTD
SiC coating

CNTD SILICON CARBIDE-HARD

Crack near coating—Graphite Interface
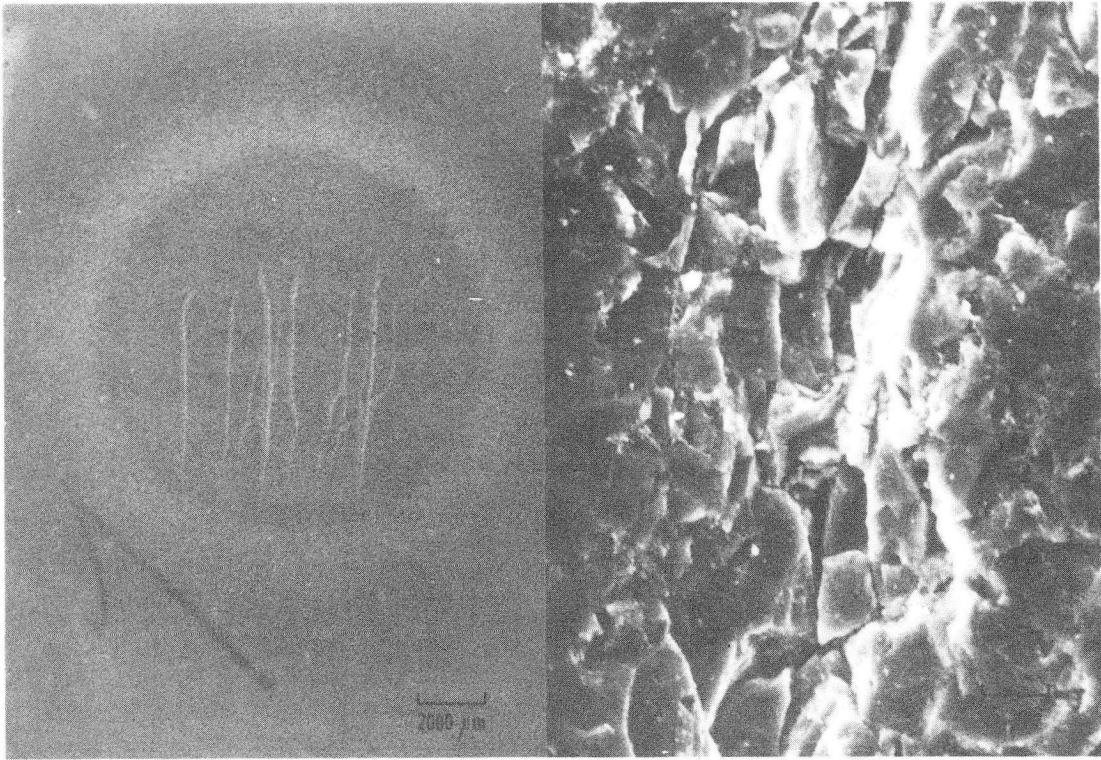
XBB 818-7789

Fig.5 Grooves in CNTD SiC near coating-
substrate interface
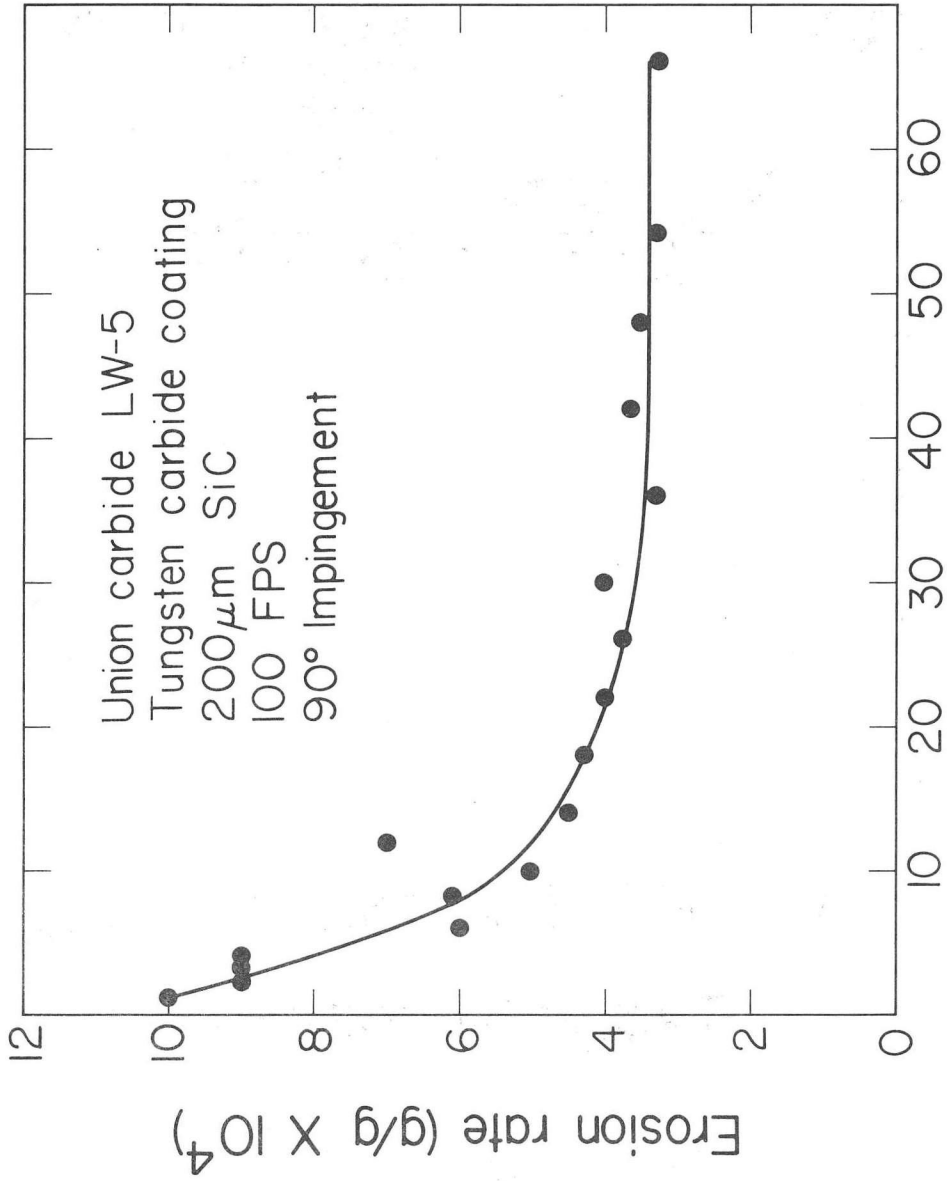
Fig.6 Incemental erosion rate of LW-5
sprayed WC
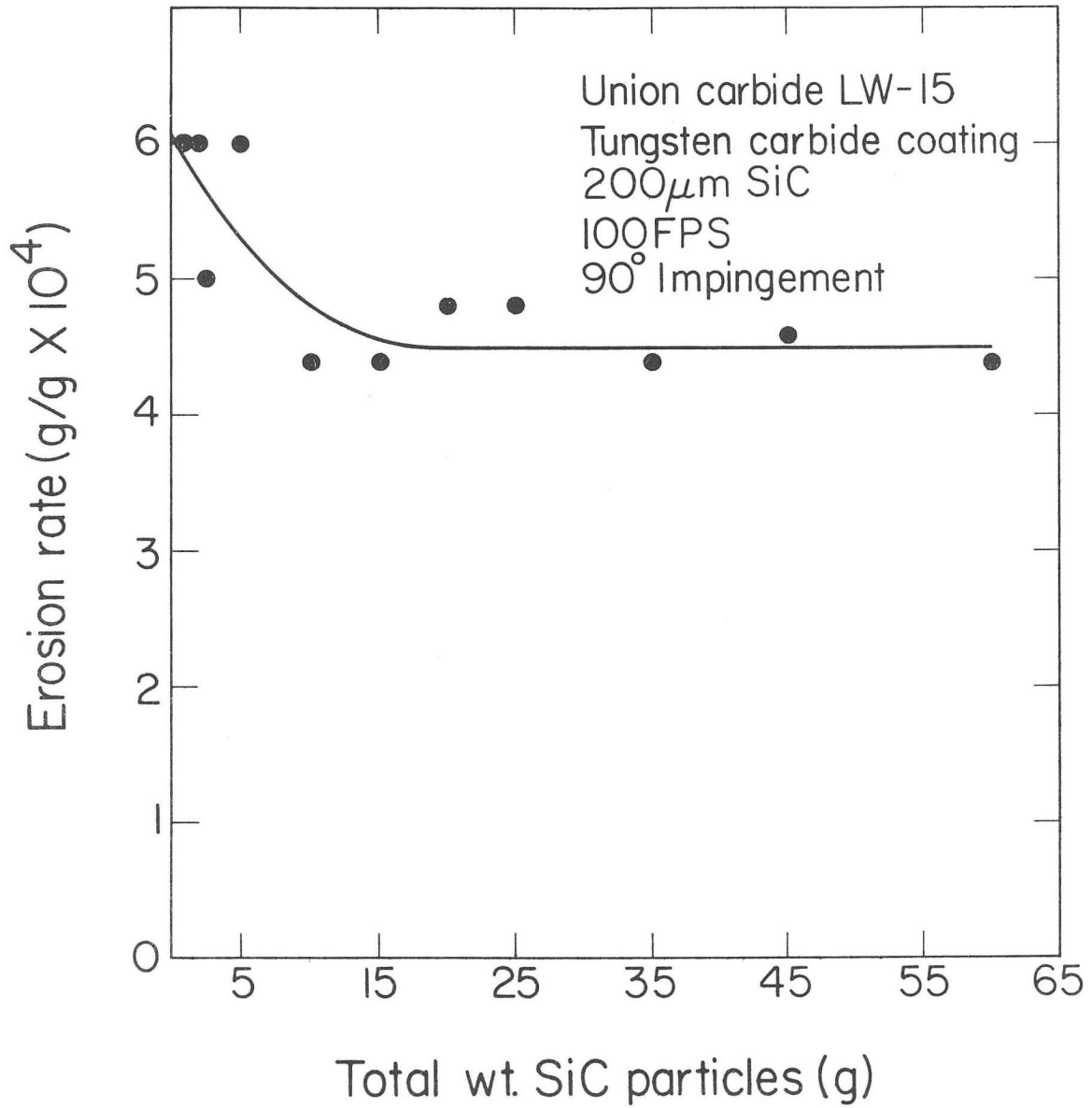
XBL 818-1186

Fig.7 Incremental erosion rate of LW-15
      sprayed WC
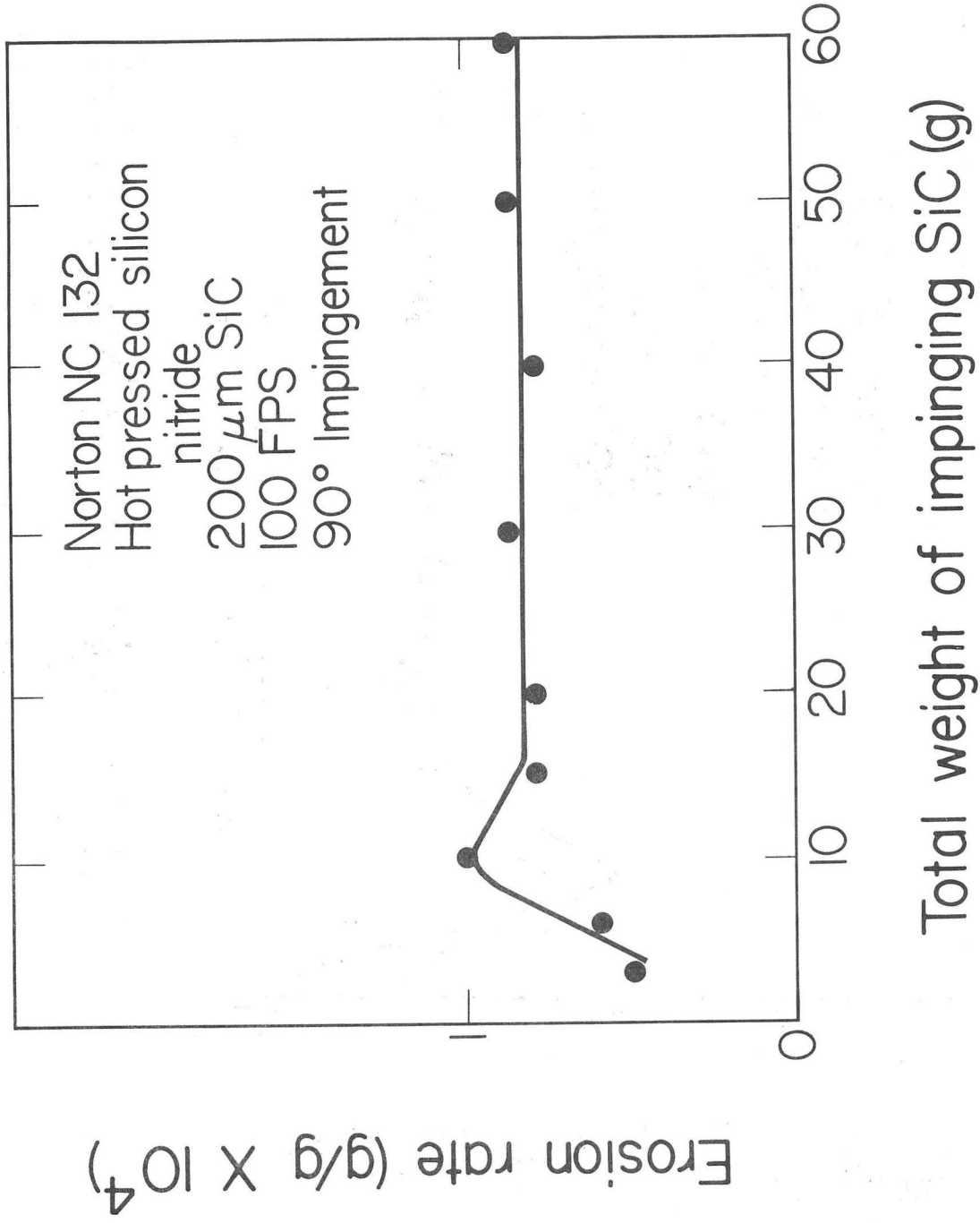
XBL 818-1180

Fig.8 Incremental erosion rate of NC-
132 hot pressed silicon

XBL 818-1181

Norton NC 203
Hot pressed silicon
carbide
200 μm SiC
100 PPS
90° Impingement

Total weight of impinging SiC (g)

Erosion rate (g/g X 10^4)
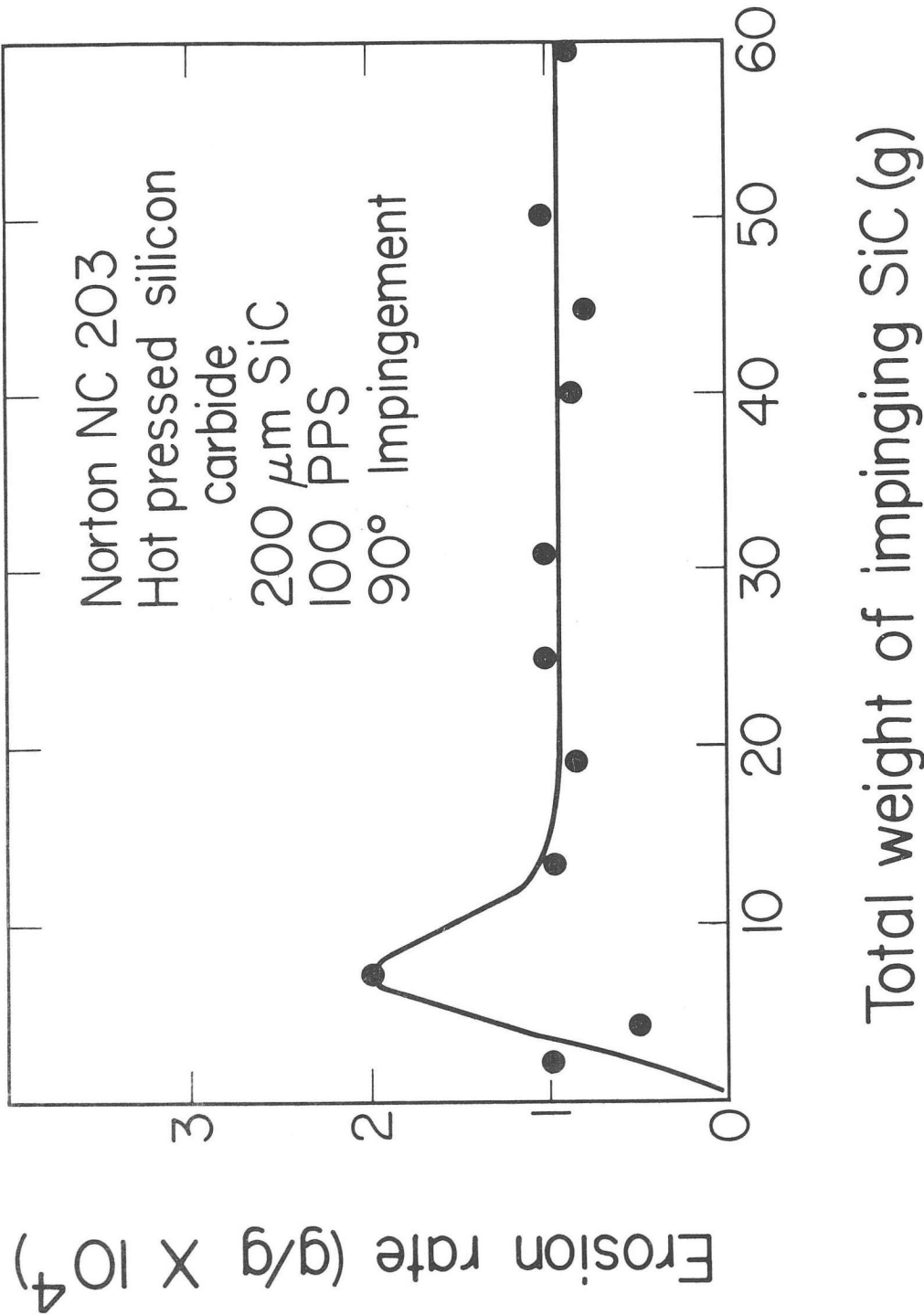
XBL 818-1175

Fig.9 Incremental erosion rate of NC-
203 hot pressed silicon carbide
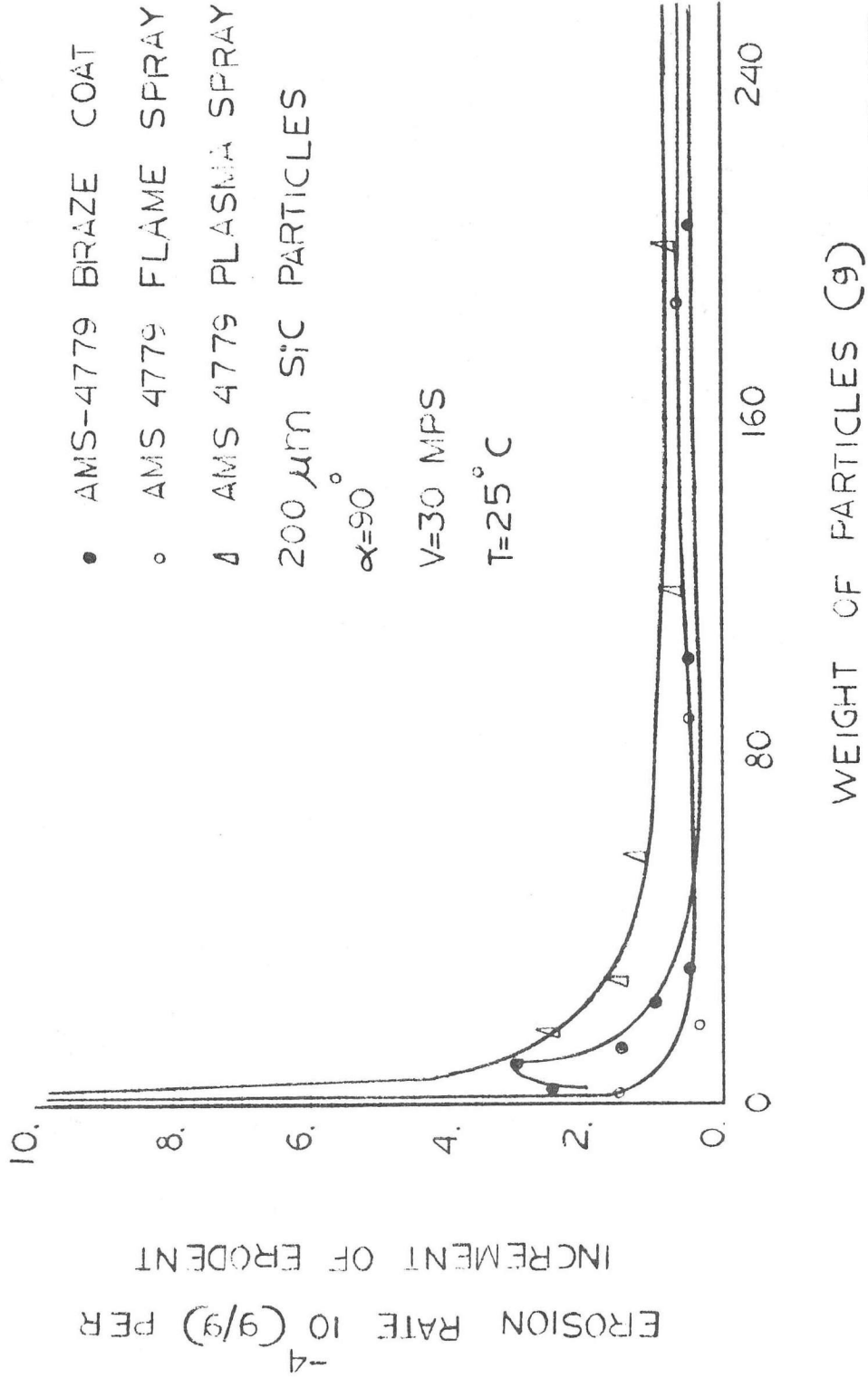
Fig.10 Erosion rate of nickel-chromium-
boron coatings

XBL 827-10758

CNTD SILICON CARBIDE

Steady State Erosion

3200 VHN   2400 VHN
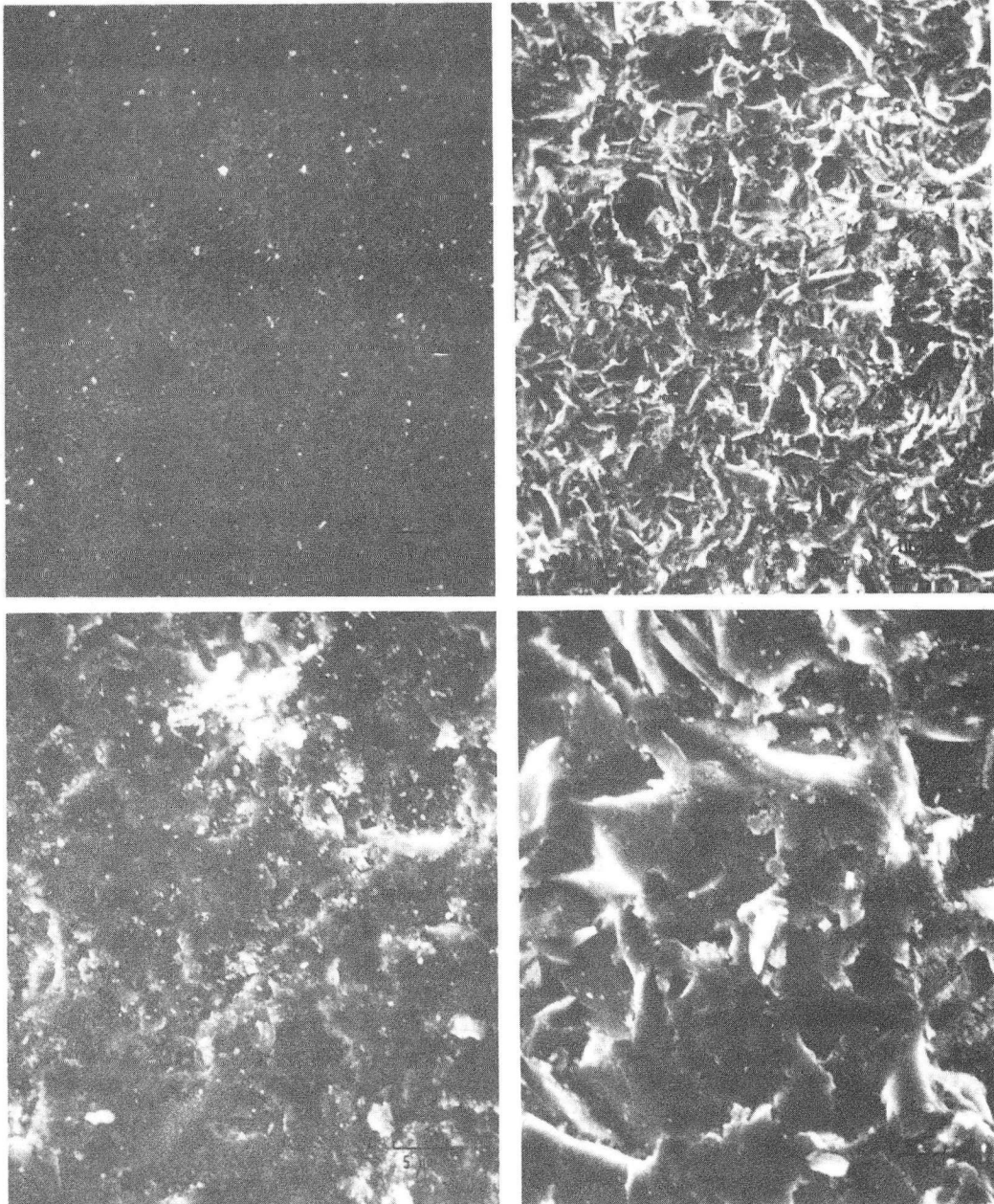
XBB 818-7787

Fig.11 CNTD silicon carbide eroded
surfaces at steady state $\alpha= 90^0$

CNTD SILICON CARBIDE

Peak Erosion

3200 VHN   2400 VHN
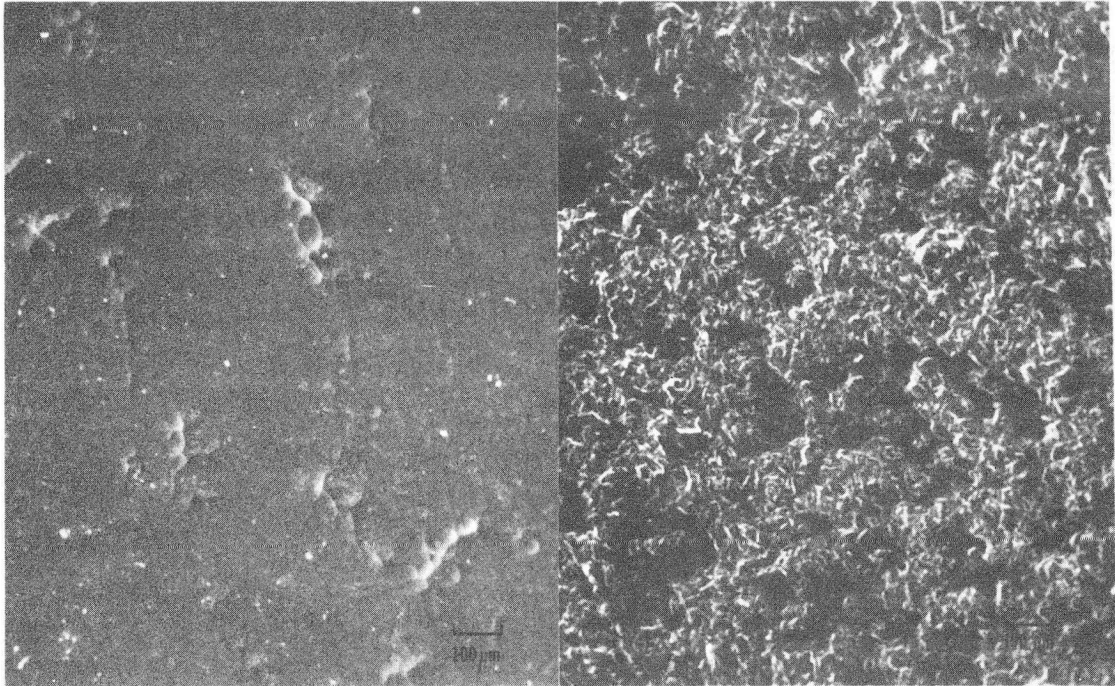
Fig.12 CNTD silicon carbide eroded
surfaces at peak erosion rate,
$\alpha = 90^{\circ}$.

XBB 818-7788
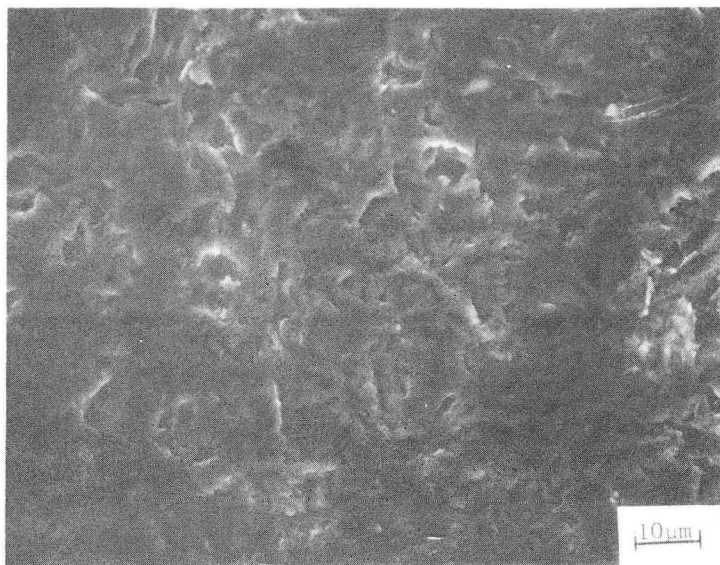
2400 VHN CNTD SiC
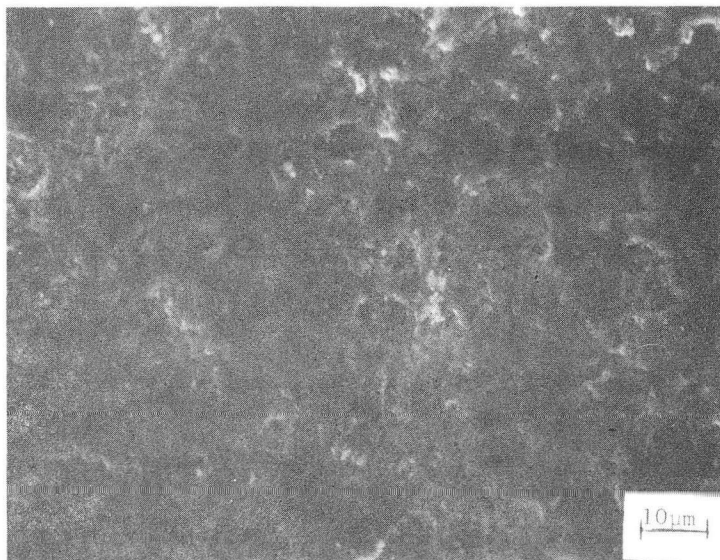
4000 VHN CNTD SiC

XBB 8210-9441

Fig.13 CNTD Silicon carbide eroded
surface at steady state, $\alpha = 30°$
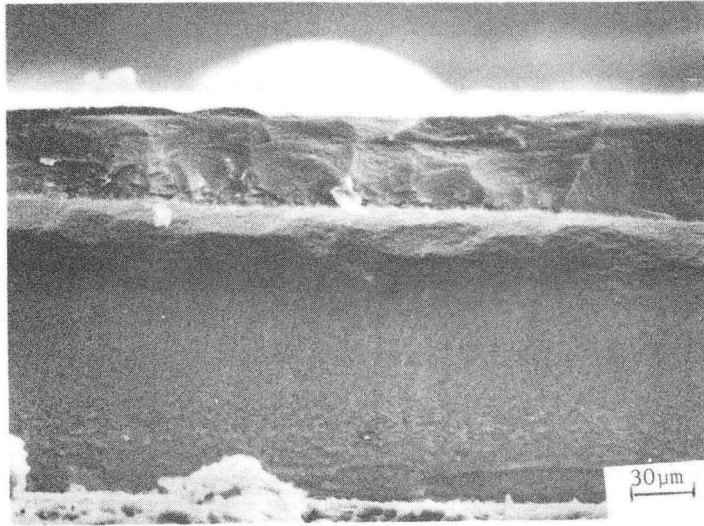
3500 VHN CNTD SiC
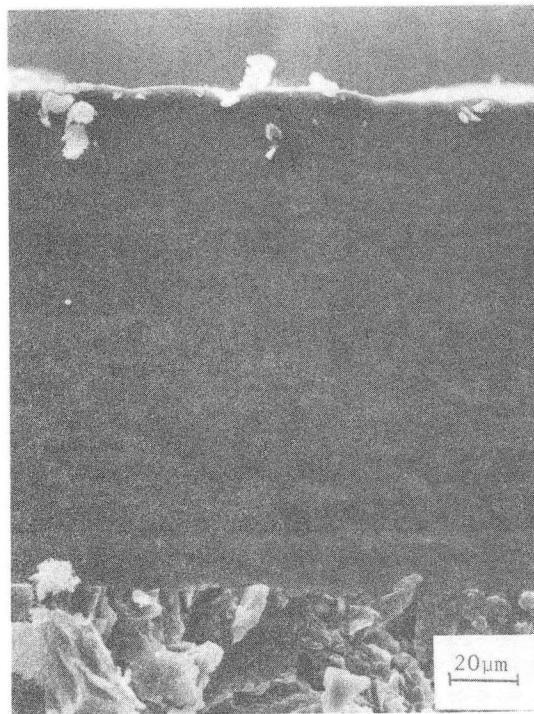
4000 VHN CNTD SiC

XBB 8210-9442

Fig.14 Fracture surface cross section
of 3500 and 4000 VHN CNTD SiC
coatings.
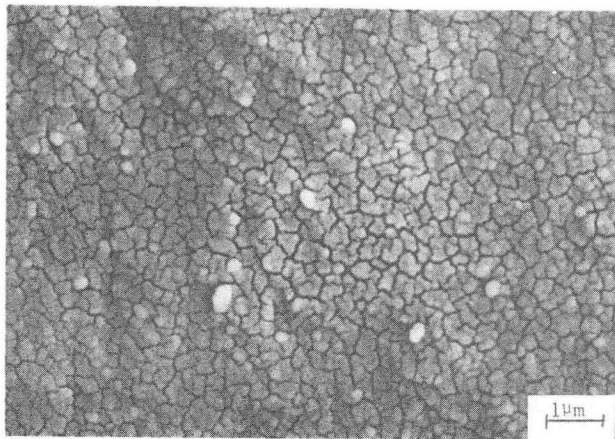
2400 VHN CNTD SiC
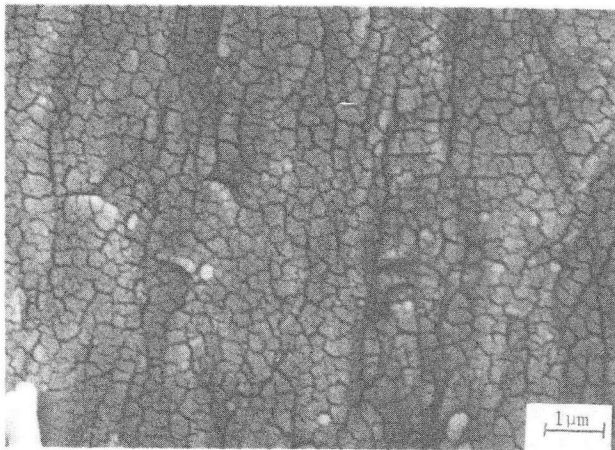
3000 VHN CNTD SiC
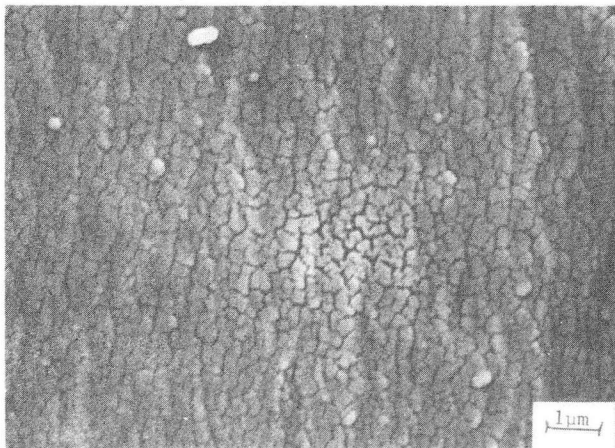
4000 VHN CNTD SiC

XBB 8210-9443

Fig.15 Fracture surfaces of 2400,3000,
4000 VHN CNTD SiC coatings.

4000 VHN CNTD SiC

0.1μm
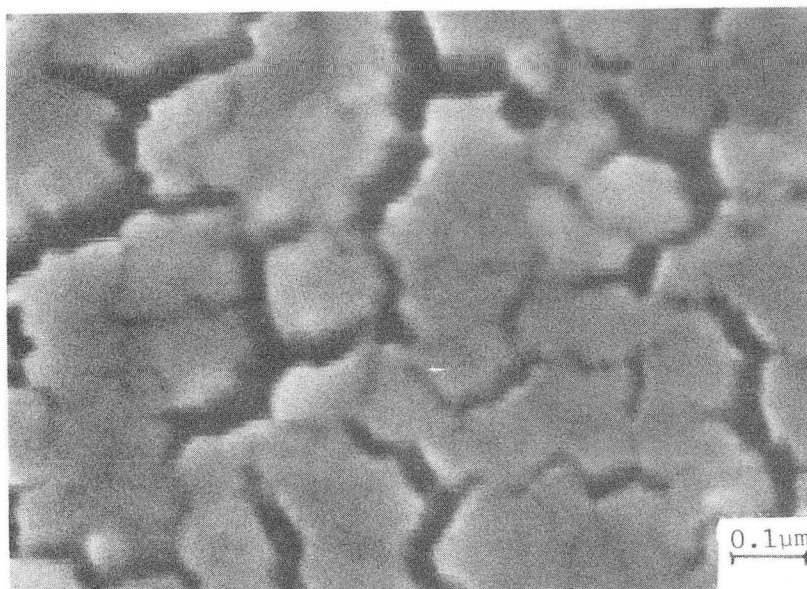
XBB 8210-9439

Fig.16 High magnification photo of
4000 VHN CNTD SiC coating
fracture sruface
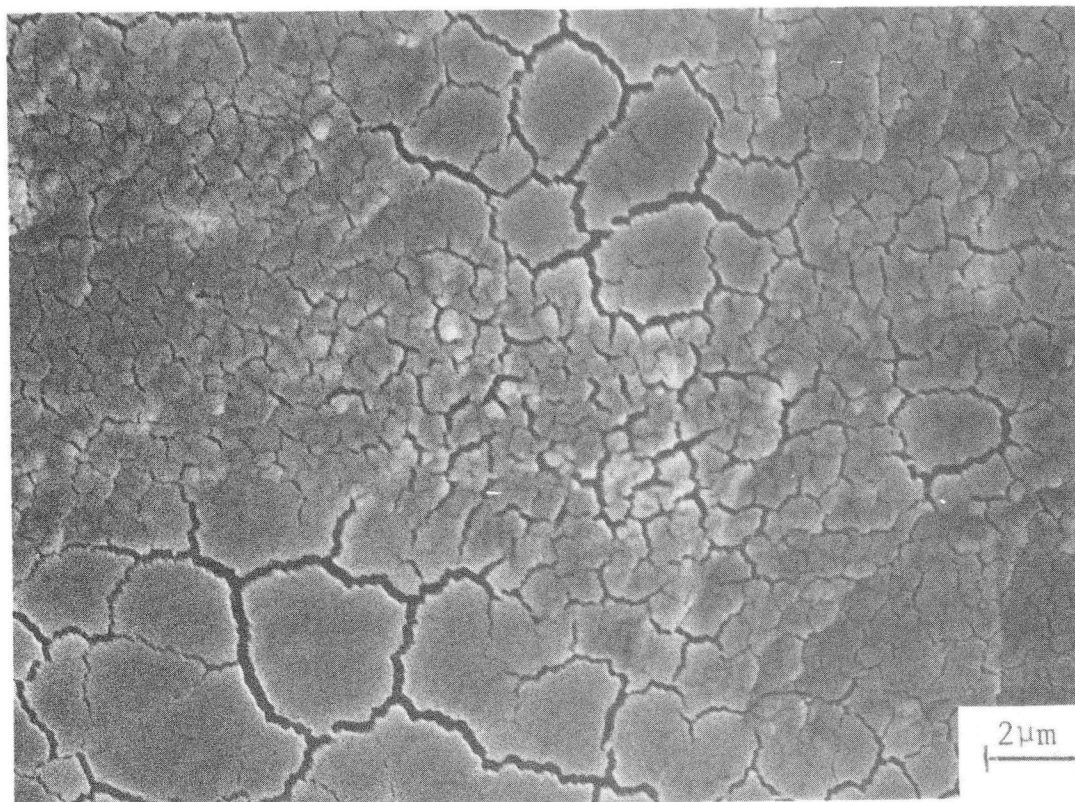
400 VHN CNTD SiC

XBB 8210-9440

Fig.17 Fracture surface of 4000 VHN
CNTD SiC coating showing
variable structure

LW-5

STEADY STATE ERODED SURFACE
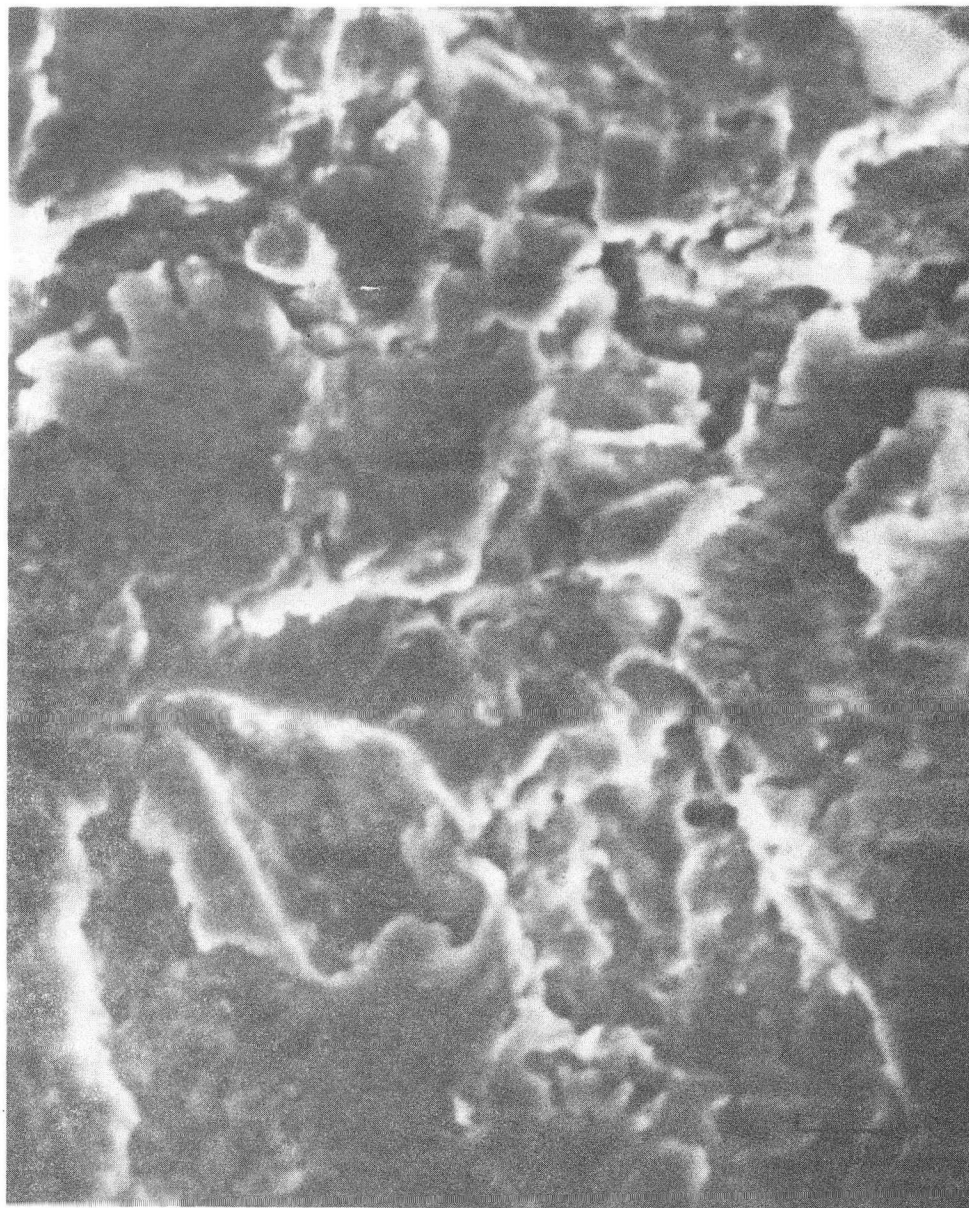
XBB 818-7790

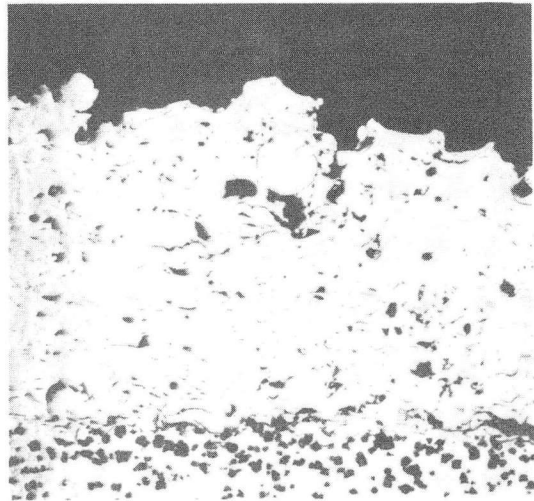Fig.18 Steady state erosion surface of
LW-5 tungsten-carbon coating

Braze Coat

40μm
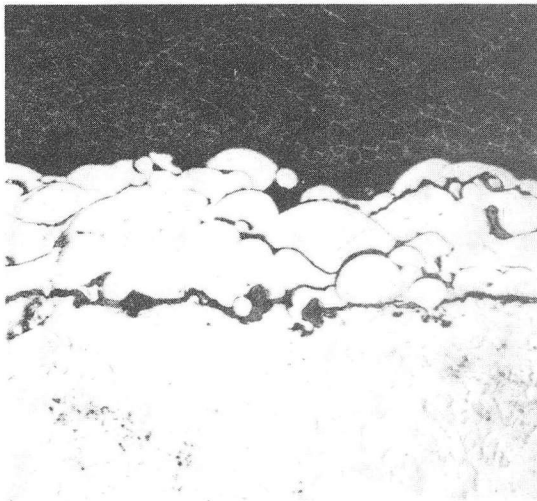
Flame Spray   50μm

Plasma Spray   50μm

XBB 827-6203

Fig.19 Cross-Sections of Uneroded
Nickel Alloy AMS-4779 Ni-B

DISTRIBUTION LIST

Wate Bakker
EPRI
Hillview Ave.
Palo Alto, CA 94303

Susan M. Benford
NASA Lewis Research Center
21000 Brookpark Rd.
Cleveland, OH 41135

Mr. R.A. Bradley, Manager
Fossil Energy Materials Program
Oak Ridge National Laboratory
P.O. Box X
Oak Ridge, TN 37830

Richard Brown
Materials Durability Division
College of Engineering
University of Delaware
Newark, DE 19711

Dr. P.T. Carlson, Task Leader
Fossil Energy Materials Program
Oak Ridge National Laboratory
P.O. Box X
Oak Ridge, TN 37830

Mr. J.P. Carr
Department of Energy, Office of Fossil Energy
FE-42, Mailstop 3222-GTN
Washington D.C. 40525

Hans Conrad
Materials Engineering Department
North Carolina State University
Raleigh, NC 27607

Mr. S.J. Dapkunas
Department of Energy, Office of Fossil Energy
Technical Coordination Staff FE-14, Mailstop C-156 GTN
Washington D.C. 40525

DOE Technical Information Center
P.O. Box 62
Oak Ridge, TN 37830

Bill Ellingson
Argonne National Laboratory
9700 South Cass Ave.
Argonne, IL 60439

Mary Ellen Gulden
Solar Turbines International
PO Box 80966
San Diego, CA 92138

Mr. J.M. Hobday
Department of Energy
Morgantown Energy Technology Center
P.O. Box 880
Morgantown, WV 26505

Mr. E.E. Hoffman, Manager
National Materials Programs
Department of Energy
Oak Ridge Operations
P.O. Box E
Oak Ridge, TN 37830

Sven Jansson
Stal-Laval Turbin AB
Finspong S-61220
Sweden

Dr. R.R. Judkins
Fossil Energy Materials Program
Oak Ridge National Laboratory
P.O. Box X
Oak Ridge, TN 37830

Thomas Kosel
University of Notre Dame
Dept. of Metallurgical Engineering & Materials Science
Box E
Notre Dame, IN 46556

Mr. E.L. Long, Jr.
Fossil Energy Materials Program
Oak Ridge National Laboratory
P.O. Box X
Oak Ridge, TN 37830

Norman H. MacMillan
Pennsylvania State University
167 Materials Research Laboratory
University Park, PA 16802

Ken Magee
Bingham-Willamette Co.
2800 N.W. Front Ave.
Portland, OR 97219

Fred Pettit
Dept. of Metallurgy and Materials Engineering
University of Pittsburgh
Pittsburgh, PA 15261

Alberto Sagües
IMMR — University of Kentucky
763 Anderson Hall
Lexington, KY 40506

Gordon Sargent
University of Notre Dame
Dept. of Metallurgical Engineering & Materials Science
Box E
Notre Dame, IN 46556

Paul Shewmon
Dept. of Metallurgical Engineering
116 W. 19th Ave.
Columbus, OH 43210

John Stringer
EPRI
3412 Hillview Avenue
P.O. Box 10412
Palo Alto, CA 94303

Widen Tabakoff
Dept. of Aerospace Engineering
University of Cincinnati
Cincinnati, OH 45221

Edward Vesely
IITRI
10 West 35th St.
Chicago, IL 60616

J.C. Williams
Dept. of Metallurgy & Materials Science
Carnegie-Mellon University
Schenley Park
Pittsburgh, PA 15213

Ian Wright
Materials Science Division
Battelle Memorial Institute
505 King Ave.
Colombus, OH 43201